BBA - Molecular Basis of Disease 1863 (2017) 2891–2903

Contents lists available at ScienceDirect

BBA - Molecular Basis of Disease

journal homepage: www.elsevier.com/locate/bbadis

Inhibition of mitochondrial fission prevents hypoxia-induced metabolic shift and cellular proliferation of pulmonary arterial smooth muscle cells

Valentina Parra[a,b], Roberto Bravo-Sagua[a,c], Ignacio Norambuena-Soto[a], Carolina P. Hernández-Fuentes[a], Andrés G. Gómez-Contreras[a], Hugo E. Verdejo[d], Rosemarie Mellado[e], Mario Chiong[a,b], Sergio Lavandero[a,b,f,*], Pablo F. Castro[d,**]

[a] Advanced Center for Chronic Diseases (ACCDiS), Facultad de Ciencias Químicas y Farmacéuticas & Facultad de Medicina, Universidad de Chile, Santiago, Chile
[b] Centro Estudios Moleculares de la Célula (CEMC), Facultad de Medicina, Universidad de Chile, Santiago, Chile
[c] Instituto de Nutrición y Tecnología de los Alimentos (INTA), Universidad de Chile, Santiago, Chile
[d] Advanced Center for Chronic Diseases (ACCDiS), División Enfermedades Cardiovasculares, Facultad de Medicina, Pontificia Universidad Católica de Chile, Santiago, Chile
[e] Facultad de Química, Pontificia Universidad Católica de Chile, Santiago, Chile
[f] Department of Internal Medicine (Cardiology Division), University of Texas Southwestern Medical Center, Dallas, TX, USA

ARTICLE INFO

Keywords:
Pulmonary artery smooth muscle cells
Trimetazidine
DRP1
Mdivi-1
Proliferation
Pulmonary artery hypertension

ABSTRACT

Chronic hypoxia exacerbates proliferation of pulmonary arterial smooth muscle cells (PASMC), thereby reducing the lumen of pulmonary arteries. This leads to poor blood oxygenation and cardiac work overload, which are the basis of diseases such as pulmonary artery hypertension (PAH). Recent studies revealed an emerging role of mitochondria in PAH pathogenesis, as key regulators of cell survival and metabolism. In this work, we assessed whether hypoxia-induced mitochondrial fragmentation contributes to the alterations of both PASMC death and proliferation. In previous work in cardiac myocytes, we showed that trimetazidine (TMZ), a partial inhibitor of lipid oxidation, stimulates mitochondrial fusion and preserves mitochondrial function. Thus, here we evaluated whether TMZ-induced mitochondrial fusion can prevent human PASMC proliferation in an *in vitro* hypoxic model. Using confocal fluorescence microscopy, we showed that prolonged hypoxia (48 h) induces mitochondrial fragmentation along with higher levels of the mitochondrial fission protein DRP1. Concomitantly, both mitochondrial potential and respiratory rates decreased, indicative of mitochondrial dysfunction. In accordance with a metabolic shift towards non-mitochondrial ATP generation, mRNA levels of glycolytic markers *HK2*, *PFKFB2* and *GLUT1* increased during hypoxia. Incubation of PASMC with TMZ, prior to hypoxia, prevented all these changes and precluded the increase in PASMC proliferation. These findings were also observed using Mdivi-1 (a pharmacological DRP1 inhibitor) or a dominant negative DRP1 K38A as pre-treatments. Altogether, our data indicate that TMZ exerts a protective role against hypoxia-induced PASMC proliferation, by preserving mitochondrial function, thus highlighting DRP1-dependent morphology as a novel therapeutic approach for diseases such as PAH.

1. Introduction

Pulmonary arteries irrigate pulmonary alveoli, where gas exchange takes place between the lungs and the bloodstream. In stark contrast to the rest of the vasculature, pulmonary arteries constrict when submitted to hypoxia, as a physiological means to distribute blood away from poorly oxygenated alveoli, thus favoring better-oxygenated ones [1,2]. Even more, chronic hypoxia increases pulmonary artery smooth muscle cell (PASMC) proliferation and resistance to cell death, thus leading to pathological narrowing of the pulmonary circulation, poor blood and tissue oxygenation, increased workload to the right heart and eventually, heart failure [3]. This mechanism is relevant for conditions such as maladaptation to hypobaric hypoxia at high altitude [2], and pulmonary hypertension (PAH) [1]. PAH is a chronic and incurable disease, characterized by excessive PASMC proliferation [3], which is aggravated by hypoxic condition [2]. During PAH onset there are

* Correspondence to: S. Lavandero, Advanced Center for Chronic Diseases (ACCDiS), Facultad Ciencias Químicas y Farmacéuticas & Facultad de Medicina, Universidad de Chile, Olivos 1007, Santiago 8380492, Chile.
** Correspondence to: P.F. Castro, Advanced Center for Chronic Diseases (ACCDiS), División de Enfermedades Cardiovasculares, Pontificia Universidad Católica de Chile, Marcoleta 367, Santiago 8330024, Chile.
E-mail addresses: slavander@uchile.cl (S. Lavandero), pcastro@med.puc.cl (P.F. Castro).

http://dx.doi.org/10.1016/j.bbadis.2017.07.018
Received 11 March 2017; Received in revised form 17 July 2017; Accepted 20 July 2017
Available online 22 July 2017

changes in the mitochondrial membrane potential ($\Delta\psi_{mt}$) and reactive oxygen species (ROS) production, which are indicative of a shift to an increased glycolytic rate with impaired mitochondrial glucose oxidation [3,4].

Several lines of evidence show that mitochondrial morphology is a key regulator of organelle function [5,6]. Mitochondria form a complex interconnected network that undergoes continuous remodeling by fusion and fission events [5,6]. Mitochondrial fusion is controlled by Mitofusin (MFN) 1 and 2, which form homo- and/or hetero-oligomers that promote outer mitochondrial membrane (OMM) fusion [6–8]. In the case of mitochondrial fission, the OMM protein FIS1 and other adaptor proteins recruit the GTPase Dynamin-related protein 1 (DRP1) to the mitochondrial surface [8–10]. At fission sites, DRP1 forms a constriction ring around mitochondria that drives organelle fragmentation coupled with GTP hydrolysis [7]. Alterations in mitochondrial morphology coincide with transitions between different respiratory states and cristae remodeling during apoptosis [5,6]. Down-regulation of MFN, for example, leads to mitochondrial fragmentation, which greatly reduces oxygen consumption and $\Delta\psi_{mt}$ [11].

Trimetazidine (TMZ) is an anti-ischemic metabolic agent, which improves myocardial glucose utilization through inhibition of fatty acid oxidation [12–14]. It promotes glucose oxidation via the Randle cycle and normalizes PASMC proliferation phenotype, thus preventing and reversing established PAH *in vivo* [3], including many downstream abnormalities such as down-regulation of Kv channels, mitochondrial hyperpolarization and ROS production [4]. Moreover, work from our laboratory has shown that low-dose of TMZ, preserves mitochondrial function in cultured cardiac myocytes via stimulation of mitochondrial elongation [15]. However, TMZ mechanism of action remains controversial, and its effects and therapeutic value on hypoxic human PASMC model are unknown.

Here, we studied TMZ protective effect via modulation of mitochondrial morphology in an *in vitro* hypoxic model. We observed that chronic hypoxia induces mitochondrial dysfunction in cultured human PASMC, concomitant with increased mitochondrial fragmentation displaying decreased MFN2 and increased DRP1 protein levels. Moreover, chronic hypoxia stimulated the expression of glycolytic genes, indicative of a metabolic switch towards extra-mitochondrial ATP generation. As expected, TMZ treatment reverted all this changes. To address whether modulation of mitochondrial morphology alone can reproduce TMZ effect, we used Mdivi-1 (Mdivi), a pharmacological DRP1 inhibitor, or a dominant negative (DN) DRP1 mutant K38A. Aside from restoring mitochondrial morphology, Mdivi and DRP1 DN also reverted the induction of glycolytic genes, preserved mitochondrial metabolism and prevented PASMC proliferation. Taken together, our results highlight mitochondrial morphology as a key target of TMZ action, thus regulating cell bioenergetics and function, which constitutes a novel therapeutic approach for diseases such as PAH.

2. Materials and methods

2.1. Materials

The antibody against DRP1 (Cat. 611112) was purchased from BD Biosciences (San Jose, CA, USA). Antibodies for MFN2 (Cat. ab50838), PINK1 (Cat. ab23707), and MTCO1 (Cat. ab90668) were from Abcam (Cambridge, UK). The antibody against HIF1α (Cat. NB100-105) was from Novus biologicals (Littleton, CO, USA). Anti-mtHSP70 antibody (Cat. MA3-028), tetramethylrhodamine methyl ester (TMRM), mitotracker green FM, Hoechst 33342, Alexa 488-conjugated anti-rabbit IgG antibody and fetal bovine serum (FBS) were from Thermo Fischer Scientific (Waltham, MA, USA). The anti-PARP (Cat. 9542) and anti-KI67 (Cat. 9129) antibodies were from Cell Signaling Technology (Danvers, MA, USA). Mdivi-1 (Mdivi), 1(2,3,4-trimethoxybenzyl) piperazine dihydrochloride (Trimetazidine or TMZ), anti-β-Tubulin antibody (Cat. T4026), carbonyl cyanide *m*-chlorophenyl-hydrazone (CCCP), and other chemicals were from Sigma Aldrich Corp (St. Louis, MO, USA). Reagents for protein assays were from Bio-Rad (Hercules, CA, USA). Generation and use of adenoviruses coding for LacZ, the dominant negative form of DRP1 (DRP1 K38A o DRP1 DN) and DRP1 wild type (DRP1 WT) have been described previously [16,17]. Briefly, cells were transduced with adenoviral vectors (multiplicity of infection, MOI; 1000) for 6 h before the hypoxia treatment. Adenovirus DRP1 DN and WT were kindly provided by Prof. Antonio Zorzano (Institute for Research in Biomedicine, Barcelona, Spain).

2.2. Cell culture and hypoxia treatment

Primary human pulmonary artery smooth muscle cells (hPASMC) cryopreserved at the end of the tertiary culture were obtained from Thermo Fischer Scientific and maintained in 231 Media supplemented with smooth muscle growth supplement (SMGS), according to provider's instructions. For all experiments, cells were seeded in SMGS-supplemented 231 media for 2 days. At that point, cells were subjected to hypoxic conditions according to experimental groups. Cells were maintained in a hypoxia chamber (100% N_2, < 1% O_2, 37 °C) for the next 2 days, and then all the experiments were performed. TMZ was dissolved in water and added at a 0–100 μM concentration 3 h prior to hypoxia as we previously described [15]. For cells treated with Mdivi, the inhibitor dissolved in DMSO was added at a 0–10 μM concentration 30 min before hypoxia. Cells were used between passages 10–18.

2.3. Western blot analysis

Once treatments were completed, cells were washed 3 times with PBS and lysed with cold NP40 buffer (Tris-HCl 100 mM pH 7.4; NaCl 300 mM; NP40 0.5% v/v) supplemented with protease and phosphatase inhibitors (Roche Applied Science, Penzberg, Germany). Homogenates were centrifuged at 14,000*g* for 10 min at 4 °C. The supernatant protein content was quantified using the Bradford-based BioRad protein assay (BioRad, Hercules, CA) and denatured in SDS buffer. Equal amounts of protein were separated by SDS–PAGE (10% polyacrylamide) and electrotransferred to nitrocellulose membranes. After blocking with 5% nonfat milk in Tris-buffered saline (pH 7.6) containing 0.1% (v/v) Tween 20 (TBST), membranes were incubated with primary antibodies at 4 °C and re-blotted with horseradish peroxidase-linked secondary antibody (1:5000 in TBST). Bioluminescence was detected using EZECL (Biological Industries, Kibbutz Beit Haemek, Israel) in a Diversity 4 System using GeneSys software and quantified by image densitometry using the ImageJ software (NIH). Protein signals were normalized by β-Tubulin levels. Uncropped Western blots of the ones used in the main Figures are showed in Figs. S3–5.

2.4. Real-time qPCR

Real-time PCR was performed with Applied Biosystems SYBR green (Thermo Fischer Scientific; Waltham, MA, USA) as previously described [18,19]. Data for each mRNA was normalized to 18S rRNA with the 2ΔΔCt method [18–20]. Primers for human mRNAs were: *HIF1α* forward 5′-GAAAGGATTACTGAGTTGATGG-3′ and reverse 5′-CAGACATATCCACCTCTTTTTG-3′; *HK2* forward 5′-CTAAACTAGACGAGAGTTTCC-3′ and reverse 5′-CATCATAACCACAGGTCATC-3′; *PFKFB2* forward 5′-TGGAGGTTAAGGTATCAAGC-3′ and reverse 5′-ATAGTTGTCTGGGTCAAGAG-3′; *SLC2A1* (GLUT1) forward 5′-CAATATGTGGAGCAACTGTG-3′ and reverse 5′-AGTAGGTGAAGATGAAGAAGAG-3′; *SLC2A4* (GLUT4) forward 5′-TCCTTCCTCATTGGTATCATC-3′ and reverse 5′-CCAAGGATGAGCATTTCATAG-3′.

2.5. Lactate assay

Lactate levels were determined in the extracellular cell media using a fluorescence-based method (L-Lactate Assay, Cayman) following the

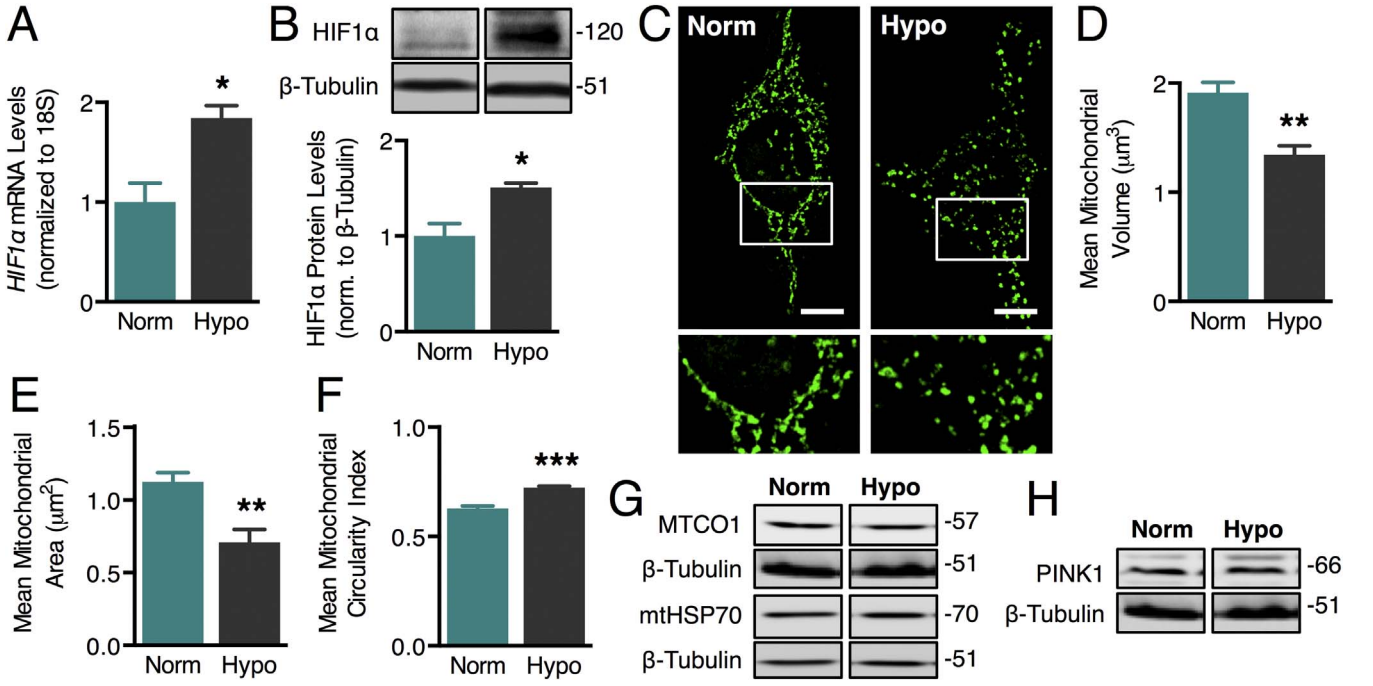

Fig. 1. Hypoxia triggers mitochondrial fragmentation in hPASMC. Cells were cultured in normoxic (Norm) or hypoxic (Hypo) conditions. A. *HIF1α* relative mRNA levels, quantified through real-time qPCR (n = 3). B. Western blot analysis of HIF1α protein levels, using β-Tubulin as a loading control (n = 4). C. Representative images of z-stack mtHSP70 immunofluorescences of hPASMC imaged via confocal microscopy. Scale bar: 10 μm. Lower panels: magnification of marked areas. D. Mean mitochondrial volume of cells imaged in C (n = 4). E. Mean mitochondrial area of cells imaged in C (n = 4). F. Mean mitochondrial circularity index of cells imaged in C (n = 4). G. Representative western blot analysis of MTCO1 and mtHSP70 protein levels, using β-Tubulin as a loading control. H. Representative western blot analysis of PINK1 protein levels, using β-Tubulin as a loading control. Bars represent mean ± SEM. *P < 0.05, **P < 0.01 & ***P < 0.001 relative to Norm, as assessed by Student's *t*-test.

manufacturer's instructions. In the assay, lactate dehydrogenase catalyzes the oxidation of lactate to pyruvate, along with the concomitant reduction of NAD^+ to NADH. NADH then reacts with the fluorescent substrate to yield a highly fluorescent product. The fluorescent product was analyzed with an excitation wavelength of 530–540 nm and an emission wavelength of 585–595 nm [21].

2.6. Mitochondrial morphology

Mitochondrial morphology analysis was performed as previously described [18,22,23]. Briefly, after treatment cells were fixed with 4% paraformaldehyde and permeabilized with 0.1% Triton X100 in ice-cold PBS, blocked in 3% bovine serum albumin PBS, and incubated with anti-mtHSP70 followed by Alexa 488 anti-mouse as primary and secondary antibodies, respectively. Confocal *Z*-stack images were obtained with a Carl Zeiss LSM-5 Pascal 5 Axiovert 200 microscope, using a Plan-Apochromat 63x/1.4 Oil DIC objective, and the LSM 5 3.2 software. Images were deconvolved and thresholded with ImageJ software (National Institutes of Health, USA), which allowed for the 3D reconstruction of the mitochondrial network of individual cells. To calculate the mean mitochondrial volume, the whole mitochondrial network was split into its composing elements (individual mitochondria), whose volumes (in μm^3) were quantified and averaged using the ImageJ plug-in 3D Object Counter. Then, all frames of the image stack were summed, resulting in the whole mitochondrial network collapsed into 1 frame. This planar image was again split into its composing elements, whose areas (in μm^2) and circularity indexes were quantified and averaged using the ImageJ function Analyze particles. Each independent experiment was performed at least four times, and 16–25 cells per condition were analyzed [22–24].

2.7. Immunofluorescence analysis of Ki67

Cells were fixed, permeabilized, blocked and incubated with a primary antibody anti-Ki67 (1:400) and a secondary anti-rabbit Alexa 488 antibody (1:600). ProLong Gold antifade with DAPI was used as mounting medium (Life Technologies, Thermo Fischer Scientific; Waltham, MA, USA). Samples were visualized under a confocal microscope. Total fluorescence was normalized to nuclei area before comparison.

2.8. Flow cytometry

After treatment, cells were loaded with either MitoTracker Green FM to determine mitochondrial mass or TMRM to evaluate $\Delta\psi_{mt}$ using the uncoupling agent CCCP as a depolarizing control. Once loaded with the respective probe, cells were trypsinized and analyzed in a FACSCAN flow cytometer. Sub-G1, G1 and S + G2 populations were also determined in hPASMC. The cells were collected and permeabilized with methanol for 24 h, treated with RNase for 1 h and then 2 μL PI (25 μg/mL) was added prior to the flow cytometry analysis. A total of five thousand cells per sample were analyzed [25,26].

2.9. Oxygen consumption

Oxygen consumption was measured by Clark oxygraphy. Cells were trypsinized, pelleted, and resuspended in PBS. The suspension was placed in a temperature-controlled chamber coupled to a Clark electrode 5331 (Yellow Springs Instruments, Yellow Springs, OH) where oxygen concentration was measured polarographically. Recording and data analysis were performed using Strathkelvin respirometry/monitoring software (North Lanarkshire, ML1 5RX). Baseline oxygen consumption was recorded for 2 min; then, oligomycin (50 nmol/L) was added and measurements continued for 2 min. Finally, CCCP (200 nmol/L) was added and measurements continued for another 2 min.

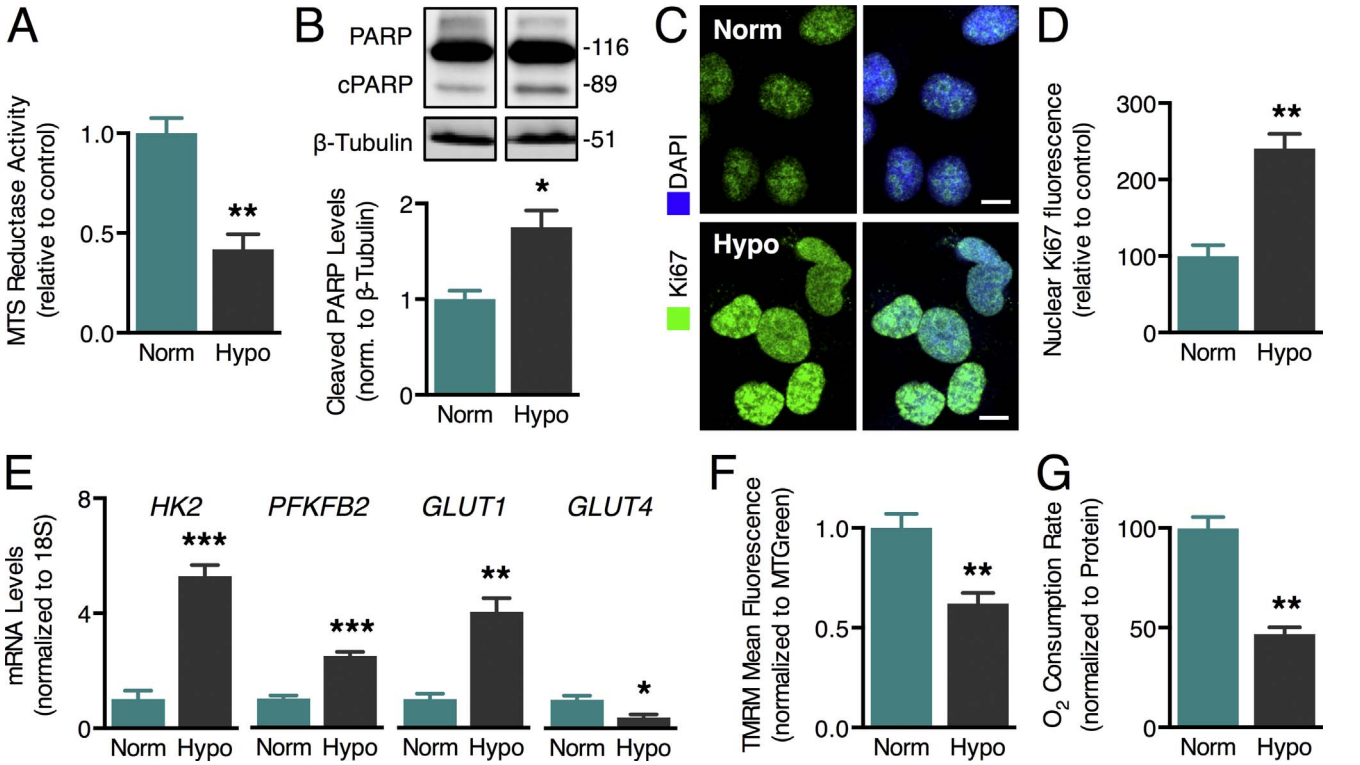

Fig. 2. Hypoxia triggers cell death, proliferation and decreases mitochondrial function in hPASMC. Cells were cultured in normoxic (Norm) or hypoxic (Hypo) conditions. A. Relative levels of MTS reductase activity, quantified through colorimetric assay (n = 4). B. Western blotting analysis of PARP, using β-Tubulin as a loading control (n = 3). C. Representative images of hPASMC probed for Ki67 (green) and nucleus (blue) imaged via confocal microscopy. Scale bar: 10 μm. D. Relative levels of nuclear Ki67 fluorescence, quantified from images as in C (n = 4). E. Relative *HK2*, *PFKFB2*, *GLUT1* and *GLUT4* mRNA levels quantified through real-time qPCR (n = 4). F. Relative $\Delta\psi_{mt}$, quantified through flow cytometry as mean TMRM fluorescence, normalized to MitoTracker Green fluorescence (n = 6). G. Relative oxygen consumption rate quantified through Clark's oxygraphy, normalized to protein content (n = 3). Bars represent mean ± SEM. *P < 0.05, **P < 0.01 and ***P < 0.001 relative to Norm, as assessed by Student's *t*-test.

2.10. Statistical analysis

Data are expressed as mean ± SEM of at least three independent experiments. For comparisons between 2 groups, results were analyzed using an unpaired two-tailed *t*-test. For experiments consisting of 4 groups, non-matching two-way ANOVA was used, followed by Holm-Sidak post-test among all experimental groups. Differences were considered significant at $P < 0.05$.

3. Results

3.1. Hypoxia stimulates mitochondrial network fragmentation in hPASMC

First, we validated our hypoxic hPASMC model by measuring the induction of Hypoxia-inducible factor 1alpha (HIF1α), master transcription factor of the cellular response to hypoxia [27,28]. After 48 h of hypoxic treatment, HIF1α mRNA and protein levels significantly increased from 1.0 ± 0.3 to 1.8 ± 0.2 and from 1.0 ± 0.3 to 1.5 ± 0.1, respectively (Fig. 1A–B). Concomitantly, mitochondrial morphology noticeably changed from connected tubes to a fragmented network, characterized by the predominance of small spherical elements (Fig. 1C). This fragmented phenotype was further evaluated by the automated quantification of individual mitochondrial volume, cross-sectional area and circularity index [15,18,22]. As expected, both mean mitochondrial volume and cross-sectional area significantly decreased from 1.9 ± 0.2 to 1.3 ± 0.2 μm^3 and from 1.1 ± 0.1 to 0.7 ± 0.2 μm^2, respectively (Fig. 1D–E), while the circularity index increased, from 0.63 ± 0.02 to 0.72 ± 0.02 suggesting the presence of more rounded elements (Fig. 1F). Importantly, the contents of two mitochondrial marker proteins, Heat-shock protein 70 (mtHSP70) and Cytochrome c oxidase 1 (MTCO1) remained unchanged, ruling out the occurrence of mitochondrial degradation (termed mitophagy) (Fig. 1G). We further corroborated this observation by assessing the protein levels of the mitophagic mediator PINK1 (Fig. 1H), which also remained unchanged after hypoxia. Altogether, these data suggest that hypoxia induces mitochondrial fragmentation in hPASMC.

3.2. Hypoxia-triggered mitochondrial network fragmentation correlates with increased hPASMC proliferation and a reduced mitochondrial metabolism

During PAH, PASMC display a proliferative phenotype that is resistant to cell death [3]. Accordingly, we measured both processes in our hypoxic system. As shown in Fig. 2, exposure to hypoxia decreased MTS reductase activity from 1.0 ± 0.2 to 0.4 ± 0.2 (Fig. 2A); and triggered a slight increase in PARP cleavage from 1.0 ± 0.2 to 1.8 ± 0.3 (Fig. 2B), both parameters indicative of increased cell death by apoptosis. Then, we measure this unexpected apoptotic increase by assessing cell cycle through flow cytometry. However, we did not find any increase in the apoptotic population, consisting in Sub-G1 cells (Fig. S1). These observations are probably due to post-apoptotic necrotic cell death [29], a process that is underestimated during the flow cytometer gating when most death cells are confused with debris. Interestingly, and despite the increased cell death, the remaining cells attached to the plate after hypoxia exhibited increased proliferation (Fig. 2C–D), evidenced as an elevated nuclear fluorescence of the proliferation marker Ki67, which is required for the effective rRNA transcription prior to mitosis [30,31]. Again, we were unable to observe this increased proliferation in our cell cycle analysis (Fig. S1). These results suggest a simultaneous induction of cell death and cell proliferation, thus increasing both apoptotic and mitotic markers in assays based in viable cells (western blot and immunofluorescence), while failing to do

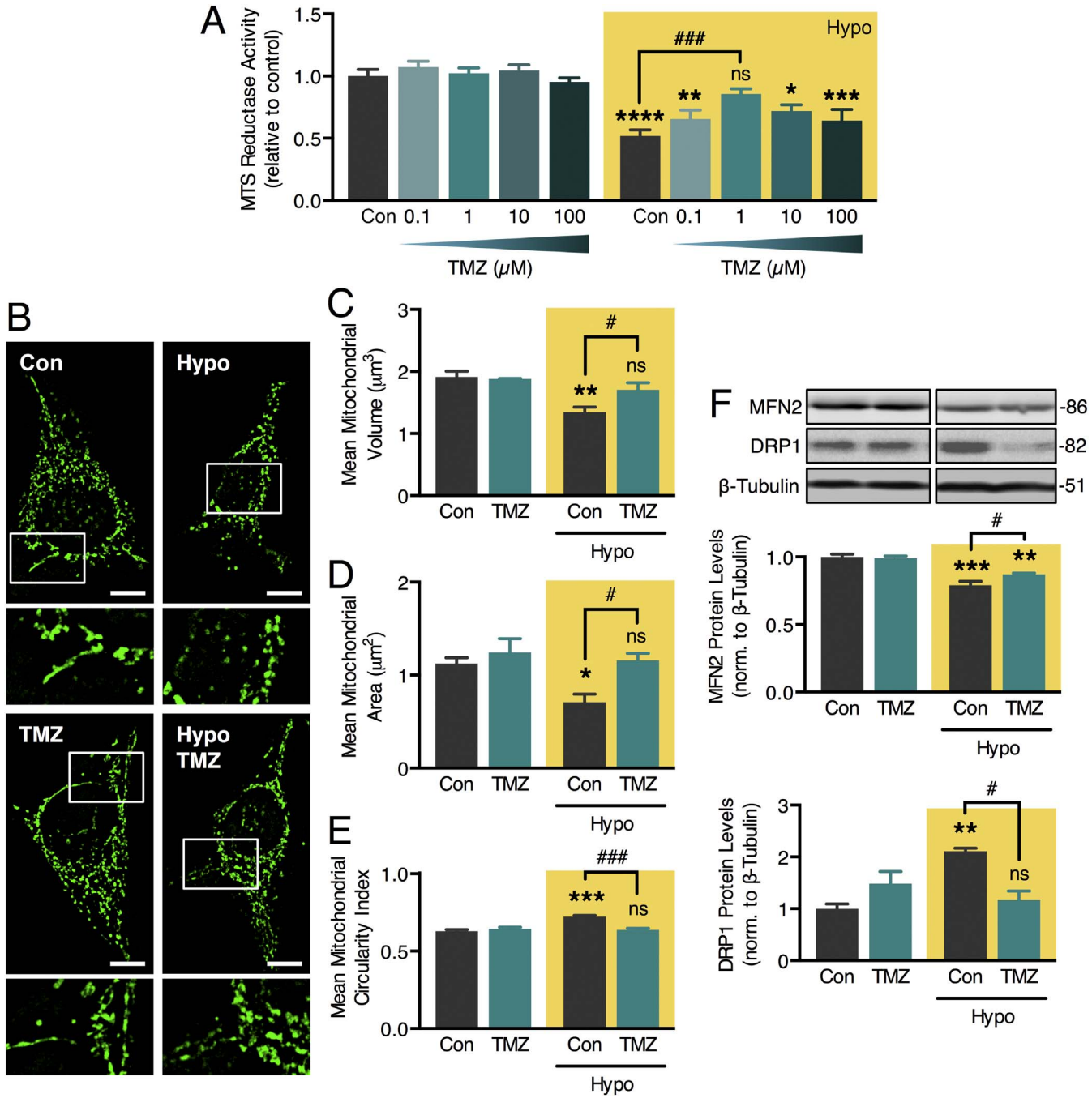

Fig. 3. TMZ prevents hypoxia-triggered mitochondrial fragmentation in hPASMC. Cells were cultured in normoxic (Norm, Con) or hypoxic (Hypo) conditions in the absence or presence of TMZ. A. Toxicity curve for increasing TMZ concentrations assayed by the relative levels of MTS reductase activity (n = 6). B. Representative images of z-stack mtHSP70 immunofluorescences of hPASMC imaged via confocal microscopy. Scale bar: 10 μm. Lower panels: magnification of marked areas. C. Mean mitochondrial volume of cells imaged in A (n = 4). D. Mean mitochondrial area of cells imaged in A (n = 4). E. Mean mitochondrial circularity index of cells imaged in A (n = 4). F. Western blot analysis of MFN2 and DRP1 protein levels, using β-Tubulin as a loading control (n = 4). Bars represent mean ± SEM. *P < 0.05, **P < 0.01, ***P < 0.001, ****P < 0.0001 & ns = non-significant relative to corresponding Con condition, while $^{\#}$P < 0.05 and $^{\#\#\#}$P < 0.001 between hypoxic conditions, as assessed by two-way ANOVA.

so in assays based in overall populations (MTS and cell cycle).

Given that hypoxic hPASMC show mitochondrial network fragmentation (Fig. 1C–E) together with decreased MTS reductase activity (Fig. 2A), we hypothesized that hypoxia diminishes mitochondrial metabolism, at expenses of anaerobic glycolysis. To test this, we evaluated the expression of four glycolytic markers through quantitative PCR [19,32]. We found that hexokinase 2 (*HK2*), 6-phosphofructo-2-kinase/fructose-2,6-biphosphatase 2 (*PFKFB2*) and solute carrier family 2 member 1 (*GLUT1*) increase their expression levels after hypoxia (Fig. 2E), whereas solute carrier family 2 member 4 (*GLUT4*) decreased (Fig. 2E). In accordance with an impaired mitochondrial function, both $\Delta\psi_{mt}$ and oxygen consumption were also significantly decreased (Fig. 2F–G). Interestingly, hypoxia not only compromised baseline mitochondrial respiration, but also mitochondrial efficiency, measured as an increase in oxygen consumption not associated with ATP synthesis (i.e. in the presence of ATP synthase inhibitor oligomycin, Fig. S2A). Furthermore, hypoxia also affected mitochondrial functional capacity, observed as a decrease in its maximal respiratory rate (i.e. in the presence of the mitochondrial uncoupler CCCP, Fig. S2A). In all, these data suggest that along with increased proliferation, hypoxia triggers

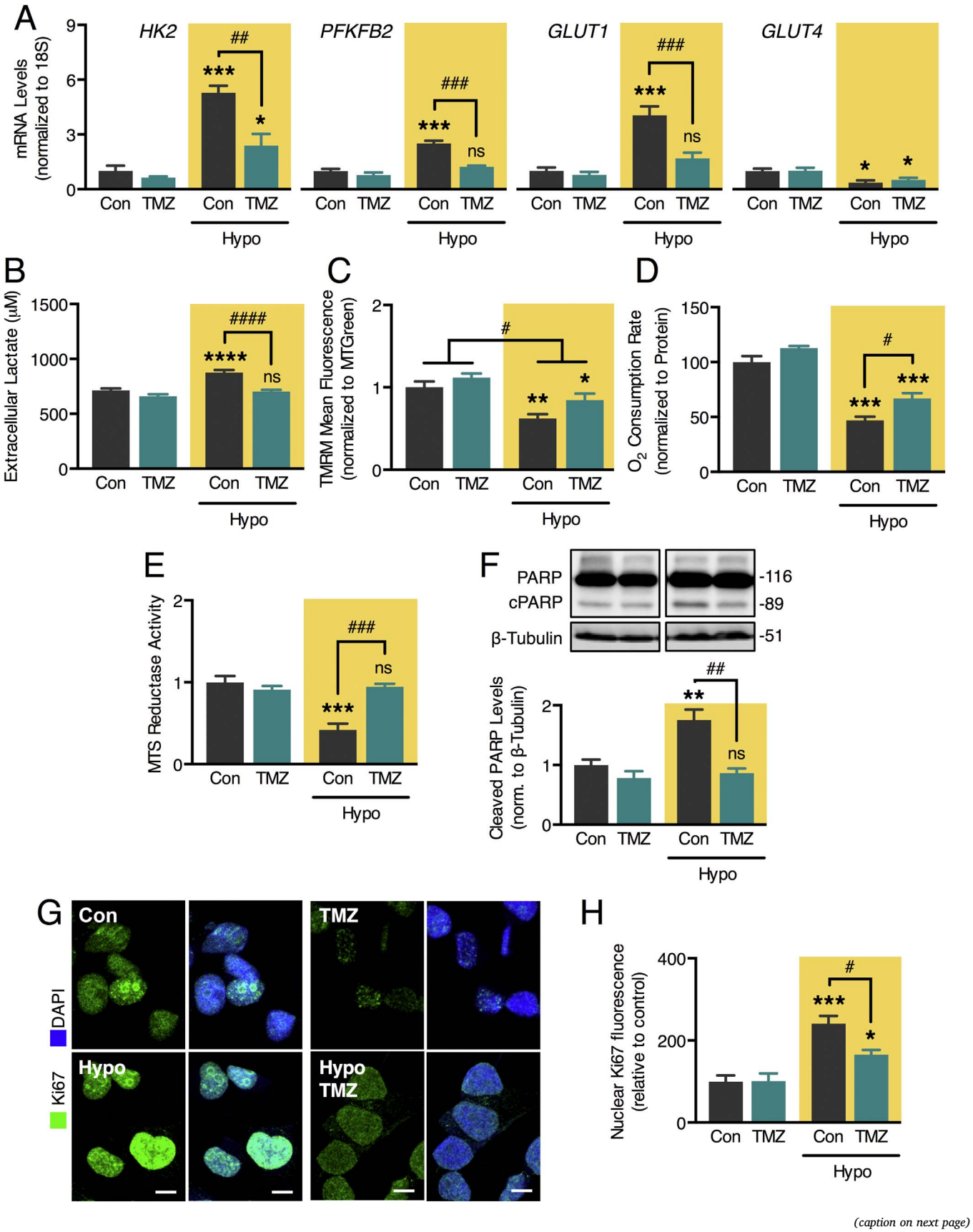

(caption on next page)

Fig. 4. TMZ inhibits the metabolic shift and proliferative phenotype induced by hypoxia in hPASMC. Cells were cultured in normoxic (Norm, Con) or hypoxic (Hypo) conditions in the absence or presence of TMZ. A. Relative *HK2*, *PFKFB2*, *GLUT1* and *GLUT4* mRNA levels quantified through real-time qPCR (n = 4). B. Extracellular lactate levels, quantified through colorimetric assay (n = 6). C. Relative $\Delta\psi_{mt}$, quantified through flow cytometry as mean TMRM fluorescence, normalized to MitoTracker Green fluorescence (n = 6). D. Relative oxygen consumption rate quantified through Clark's oxygraphy, normalized to protein content (n = 3). E. Relative levels of MTS reductase activity, quantified through colorimetric assay (n = 4). F. Western blotting analysis of PARP, using β-Tubulin as a loading control (n = 3). G. Representative images of hPASMC probed for Ki67 (green) and nucleus (blue) imaged via confocal microscopy. Scale bar: 10 μm. H. Relative levels of nuclear Ki67 fluorescence, quantified from images as in F (n = 4). Bars represent mean ± SEM. *P < 0.05, **P < 0.01, ***P < 0.001, ****P < 0.0001 & ns = non-significant relative to corresponding Con condition, while #P < 0.05, ##P < 0.01, ###P < 0.001 & ####P < 0.0001 between hypoxic conditions, as assessed by two-way ANOVA.

mitochondrial dysfunction in hPASMC, which is characterized by increased mitochondrial fission and a decreased mitochondrial metabolism.

3.3. TMZ prevents the hypoxia-triggered mitochondrial network fragmentation in hPASMC

To evaluate TMZ effects in our hypoxic hPASMC model, we titrated TMZ concentration under normoxic and hypoxic conditions. We observed that 3 h of TMZ 1 μM was the most effective concentration for preventing the hypoxia-induced decrease in MTS activity described after hPASMC hypoxia (Fig. 3A), which agrees with our previous findings in neonatal cardiomyocytes [15]. Moreover and as we expected, TMZ treatment prevented the mitochondrial fragmentation induced by 48 h of hypoxia (Fig. 3A), which is shown as a recovery of the mean mitochondrial volume, mean mitochondrial area and circularity index (Fig. 3C–E). Indeed, hypoxia-dependent mitochondrial network fragmentation was accompanied by a slight decrease in the levels of the fusion protein MFN2, and an important increase in the levels of the fission protein DRP1. Besides, the changes in MFN2 were partially inhibited by TMZ pre-treatment, while the increase in DRP1 was completely abolished (Fig. 3F).

3.4. TMZ inhibits hypoxia-dependent metabolic shift and proliferative phenotype in hPASMC

Similarly to its effect on mitochondrial fragmentation, TMZ prevented the hypoxia-induced increases in the glycolytic markers *HK2*, *PFKFB2* and *GLUT1* (Fig. 4A), without any effect on *GLUT4* levels (Fig. 4A); thus suggesting that its reduction after hypoxia might be a compensatory response to the increased *GLUT1* expression. Accordingly, hypoxia raised the extracellular levels of the glycolysis-associated metabolite lactate, an effect that was prevented by TMZ pre-treatment (Fig. 4B).

Together with the above described glycolytic effects, mitochondrial dysfunction was also prevented by TMZ, observed as a global increase in $\Delta\psi_{mt}$ of TMZ-treated cells relative to untreated cells (Fig. 4C), as well as a partial restoration of baseline, non-ATP related and maximal oxygen consumption rates (Fig. 4D and S2A). Similarly, the drop in MTS reductase activity was completely abolished (Fig. 4E), as well as PARP cleavage (Fig. 4F). Finally, and most importantly, the higher nuclear presence of Ki67 triggered by hypoxia was also hindered by TMZ pretreatment (Fig. 4G–H). These data suggest that together with preserving mitochondrial morphology after hypoxia, TMZ also protects mitochondrial function and averts proliferation induction in hPASMC.

3.5. Inhibition of mitochondrial fission abrogates hypoxia-dependent mitochondrial fragmentation, the increased glycolytic metabolism and hPASMC proliferation

To test the importance of mitochondrial morphology in TMZ actions, we assessed the effect of Mdivi, a DRP1 inhibitor, in the metabolism and proliferation of hPASMC. First, we established a non-toxic concentration for the 48 h of treatment with Mdivi necessary for achieving protection in front of the hypoxia challenge (Fig. 5A) and next, with that concentration, we proceed to evaluate mitochondrial morphology. As we expected, Mdivi (1 μM) avoids hypoxia-triggered mitochondrial fission, assessed as the quantification of the mean mitochondrial volume, area, and circularity index (Fig. 5B–E). Moreover, Mdivi also impeded the hypoxia-induced metabolic shift in hPASMC, observed as increases in the glycolytic markers *HK2*, *PFKFB2* and *GLUT1* (Fig. 5F). Similarly to TMZ, Mdivi also did not have any effect on GLUT4 levels (Fig. 5F). Parallel, Mdivi also prevented the elevation of lactate levels and preserved the mitochondrial function, observed as the partial restoration of basal, non-ATP related and maximal oxygen consumption rates (Fig. 5G–H and S2B). Finally and more important, Mdivi recapitulated the effects of TMZ on the nuclear fluorescence of Ki67 in hypoxic hPASMC, associated with the proliferative phenotype (Fig. 5I–J).

Finally, and due that recently Mdivi has been described as an inhibitor of mitochondrial complex I [33], we use two adenoviral vectors coding for the wild type (WT) and a dominant negative form of DRP1 (DRP1 K38A) to validate our findings [16,17]. As shown in Fig. 6A–E, wild-type DRP1-transduced cells in normoxic condition displayed a tendency for mitochondrial fragmentation, which was significant in terms of the mitochondrial circularity index. DRP1 DN, in turn, favored mitochondrial elongation in normoxic conditions, compared with LacZ and wild-type DRP1. When exposed to hypoxic condition, both LacZ- and wild-type DRP1-transduced cells underwent mitochondrial fragmentation, which was completely prevented by DRP1 DN. Concomitantly; wild-type DRP1 induced a higher proliferative state compared to DRP1 DN expression, even in normoxic conditions (Fig. 7A–B). Likewise, hypoxia-induced hPASMC proliferation was exacerbated by wild-type DRP1, while it was completely prevented by DRP1 DN (Fig. 7A–B). Remarkably, cells with higher proliferative state correlated with augmented mitochondrial fragmentation.

4. Discussion

In this work, we show that mitochondrial fusion triggered by the fatty acid oxidation inhibitor TMZ, the pharmacological DRP1 inhibitor Mdivi, or transduction with a mutant DRP1 all prevent mitochondrial dysfunction induced by hypoxia in hPASMC, avoiding the increase in glycolytic markers and restoring the non-proliferative phenotype that characterizes these cells (Fig. 8). Previous work showed that PASMC from PAH patients exhibit enhanced glycolytic state with decreased mitochondrial metabolism, which closely resembles the behavior of cancer cells [34], showing an apoptotic-resistant, proliferative phenotype that leads to vascular thickening and occlusion, increased pulmonary resistance and ultimately right heart failure [34].

The seminal paper of Sutendra et al. was inspired by the similitudes between PASMC in PAH and cancer cells. They also showed that when the relationship between glycolysis (GLY) and glucose oxidation (GO) was restored, PASMC recovered their normal phenotype [4]. However, the mechanisms leading to this cancer-like metabolic shift are still largely unknown. One proposed mechanism links hypoxia-induced endoplasmic reticulum (ER) stress and mitochondrial dysfunction by the disruption of ER-mitochondria contacts by the reticulon ER protein Nogo. The use of a chemical chaperone decreased Nogo expression, increased mitochondrial calcium levels, decreased Δψmt, increased mROS and also reduced proliferation and induced apoptosis [35]. In this paper, we contribute to this discussion by showing that pharmacological and genetic interventions that prevent mitochondrial fragmentation can directly restore normal PASMC mitochondrial function

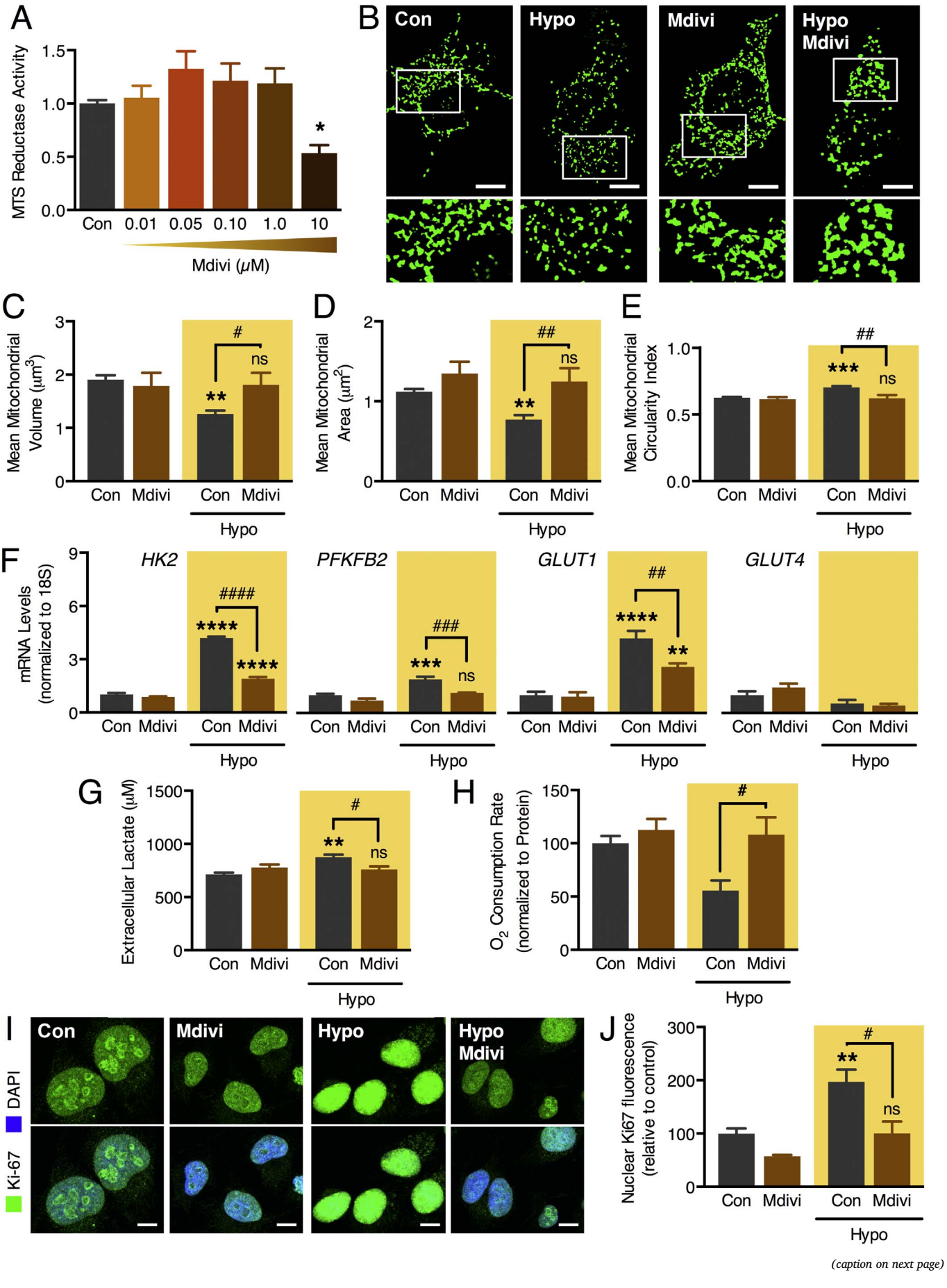

(caption on next page)

Fig. 5. Mdivi prevents the mitochondrial dysfunction and higher proliferation induced by hypoxia in hPASMC. Cells were cultured in normoxic (Norm, Con) or hypoxic (Hypo) conditions in the absence or presence of Mdivi. A. Toxicity curve for increasing Mdivi concentrations assayed by the relative levels of MTS reductase activity (n = 4). B. Representative images of z-stack mtHSP70 immunofluorescences of hPASMC imaged via confocal microscopy. Scale bar: 10 μm. Lower panels: magnification of marked areas. C. Mean mitochondrial volume of cells imaged in B (n = 3). D. Mean mitochondrial area of cells imaged in B (n = 3). E. Mean mitochondrial circularity index of cells imaged in B (n = 3). F. Relative *HK2*, *PFKFB2*, *GLUT1* and *GLUT4* mRNA levels quantified through real-time qPCR (n = 4). G. Extracellular lactate levels, quantified through colorimetric assay (n = 6). H. Relative oxygen consumption rate quantified through Clark's oxygraphy, normalized to protein content (n = 3). I. Representative images of hPASMC probed for Ki67 (green) and nucleus (blue) imaged via confocal microscopy. Scale bar: 10 μm. J. Relative levels of nuclear Ki67 fluorescence, quantified from images as in F (n = 3). Bars represent mean ± SEM. $^{**}P < 0.01$, $^{***}P < 0.001$, $^{****}P < 0.0001$ & ns = non-significant relative to corresponding Con condition, while $^{\#}P < 0.05$, $^{\#\#}P < 0.01$, $^{\#\#\#}P < 0.001$ & $^{\#\#\#\#}P < 0.0001$ between hypoxic conditions, as assessed by two-way ANOVA.

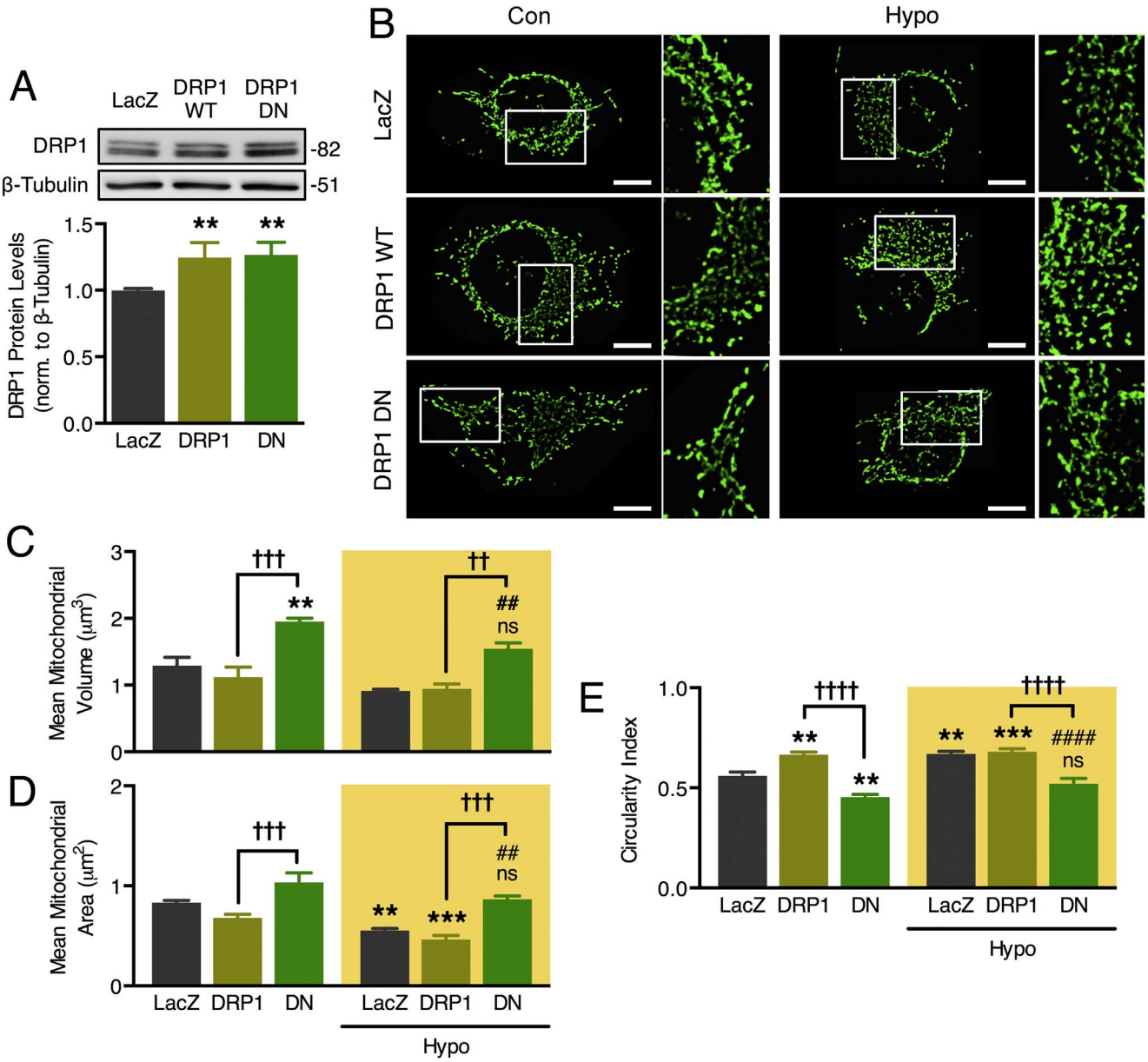

Fig. 6. The expression of a dominant negative form of DRP1 prevents the hypoxia triggered mitochondrial fragmentation induced in hPASMC. A. Western blot analysis of DRP1 protein levels, using β-Tubulin as a loading control in LacZ and DRP1 K38A (DRP1 DN) hPASMC (n = 4). B. Cells were cultured in normoxic (Norm, Con) or hypoxic (Hypo) conditions in the presence of an adenovirus encoding for LacZ, DRP1 wild type (DRP1 WT) or DRP1 DN. Then, Representative images of z-stack mtHSP70 immunofluorescences of hPASMC imaged via confocal microscopy were obtained. Scale bar: 10 μm. Right panels: magnification of marked areas. C. Mean mitochondrial volume of cells imaged in B (n = 3). D. Mean mitochondrial area of cells imaged in B (n = 3). E. Mean mitochondrial circularity index of cells imaged in B (n = 3). Bars represent mean ± SEM. $^{**}P < 0.01$, $^{***}P < 0.001$, $^{****}P < 0.0001$ & ns = non-significant relative to corresponding Con condition, $^{\#\#}P < 0.01$ & $^{\#\#\#\#}P < 0.0001$ between hypoxic conditions, while $^{\dagger}P < 0.05$, $^{\dagger\dagger}P < 0.01$, $^{\dagger\dagger\dagger}P < 0.001$ & $^{\dagger\dagger\dagger\dagger}P < 0.0001$ relative to DRP1 WT, as assessed by two-way ANOVA.

and proliferative phenotype. This study reinforces previous work describing that hypoxia induces mitochondrial fragmentation in hPASMC [36]. Said changes can be interpreted as part of the mitochondrial redistribution required for cell proliferation [37]. Indeed, we rule out that this mitochondrial fragmentation preludes mitophagic degradation, evidenced by the lack of changes in mitochondrial markers and PINK1 levels (Fig. 1G–H).

Metabolic modulation of PASMC is an attractive therapeutic target, and the use of TMZ as adjuvant therapy for PAH has already been assessed by at least one randomized clinical trial (NCT02102672). In

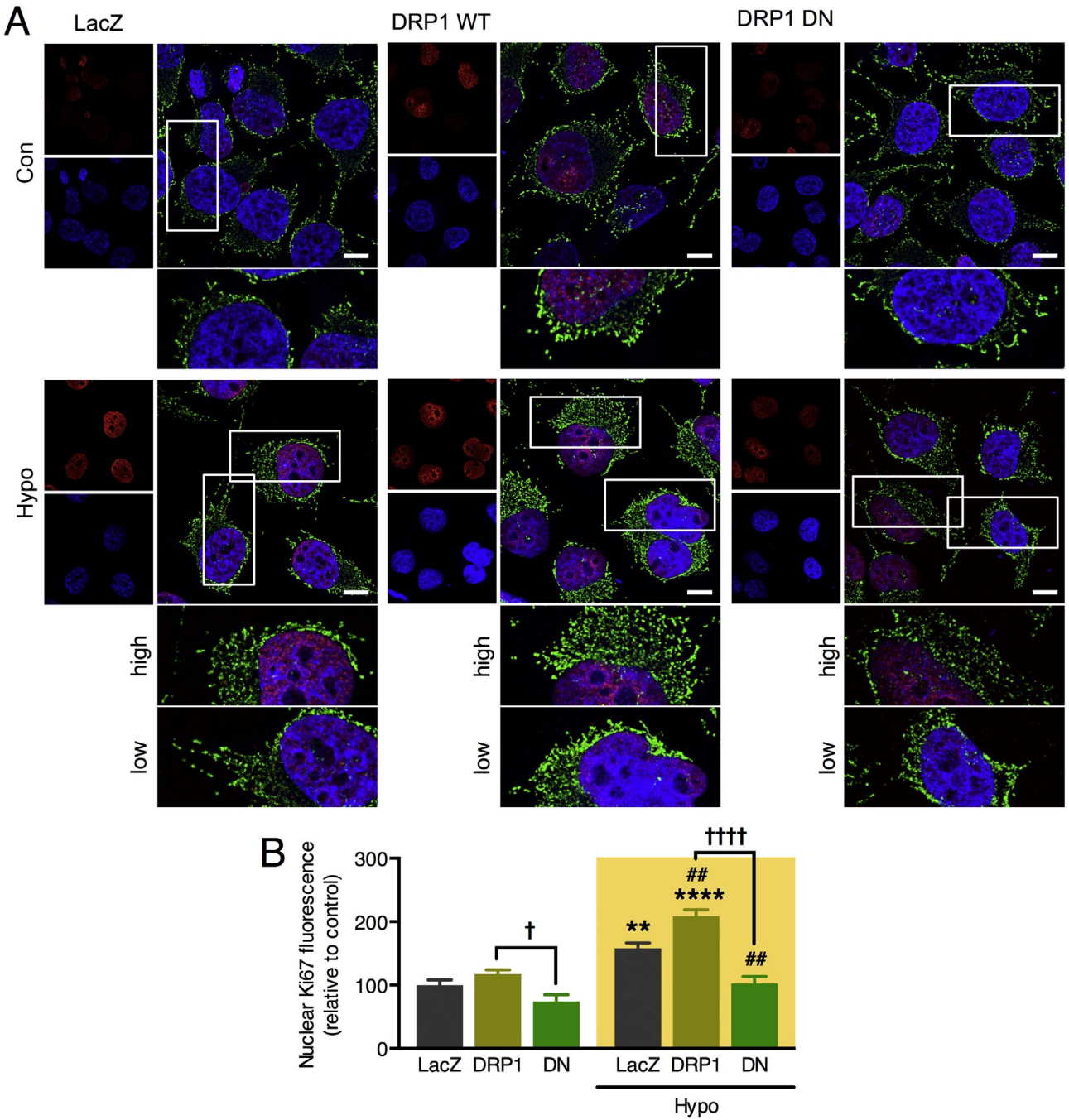

Fig. 7. DRP1 dominant negative (DRP1 K38A or DN) prevents the higher proliferation induced by hypoxia in hPASMC. A. Cells were cultured in normoxic (Norm, Con) or hypoxic (Hypo) conditions in the presence of an adenovirus encoding for LacZ, DRP1 WT or DRP1 DN. Representative images of hPASMC probed for Ki67 (red), mtHSP70 (green) and nucleus (blue) imaged via confocal microscopy. Lower panels: magnification of marked areas. Given their homogeneity, only 1 magnification is shown for cells in normoxic conditions; in contrast, different cells in hypoxic conditions display either lower of higher levels of nuclear Ki67 fluorescence. Scale bar: 10 μm. B. Relative levels of nuclear Ki67 fluorescence, quantified from images as in A (n = 4). Bars represent mean ± SEM. $^{**}P < 0.01$ & $^{****}P < 0.0001$ relative to corresponding Con condition, $^{\#\#}P < 0.01$ between hypoxic conditions, while $^{\dagger}P < 0.05$ & $^{\dagger\dagger\dagger\dagger}P < 0.0001$ relative to DRP1 WT, as assessed by two-way ANOVA.

animal PAH models, trimetazidine (TMZ) treatment decreases PASMC proliferation and restores apoptotic susceptibility, thereby reducing pulmonary vasoconstriction [4]. The proposed mechanism for TMZ action is an antagonistic effect on fatty acid metabolism, resulting in increased glucose utilization for ATP production [12] probably through partial inhibition of mitochondrial β-oxidation [13] and mitochondrial lipid uptake [14]. Aside from shifting substrate preference, TMZ has also been shown to decrease mitochondrial respiration during cardiac ischemia [38]. There, it exerts a cardioprotective role through decreased oxygen consumption and ROS production [39], thus allowing for the conservation of a healthy $\Delta\psi_{mt}$ [40]. In our hands, TMZ not only restored mitochondrial function, but also reverted mitochondrial fragmentation, thereby reinforcing the concept that mitochondrial morphology and function are highly interdependent [41]. As expected, hypoxia leads to mitochondrial network fission accompanied by a decrease in the fusion-related protein MFN2, and an important increase in the fission-related protein, DRP1. However, the reversal of mitochondrial fragmentation elicited by TMZ was accompanied by rather small changes in the MFN2 protein levels, but at the DRP1 protein levels, a complete recovery was seen. Consequently, the specific DRP1 inhibitor,

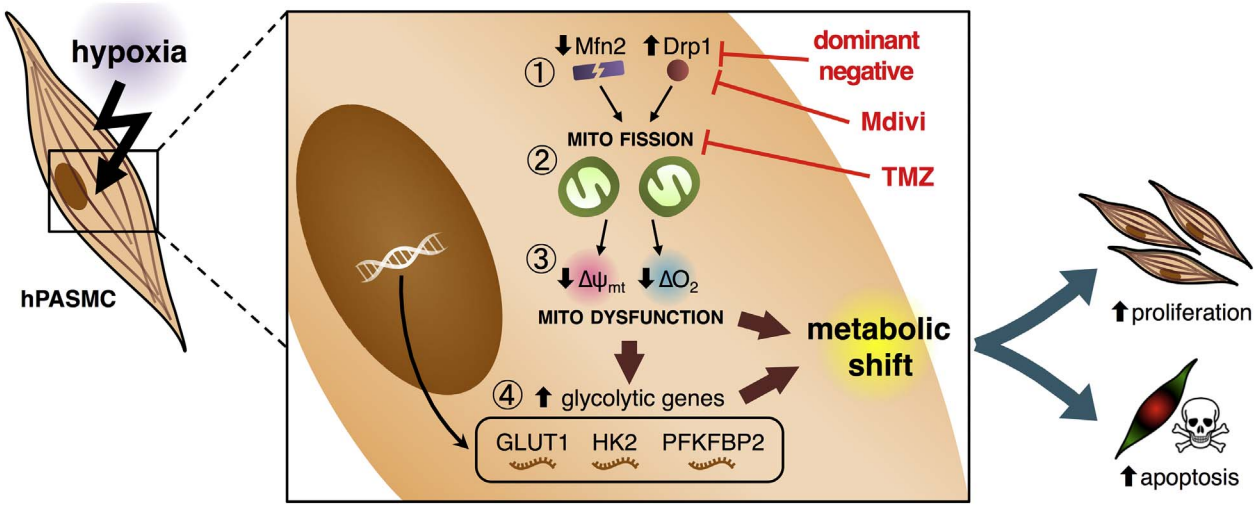

Fig. 8. Proposed Model: Inhibition of mitochondrial fragmentation prevents hypoxia-triggered glycolytic switch and mitochondrial dysfunction in hPASMC, thus restoring cell death and proliferation induction to basal levels. In hPASMC, hypoxia induces, along with HIF1α expression, the up-regulation of the glycolytic genes hexokinase 2 (HK2), phosphofructokinase 2 (PFKFB2) and glucose transporter 1 (GLUT1). These changes correlate with mitochondrial fragmentation (driven by DRP1 up-regulation and MFN2 down-regulation), decrease in both mitochondrial potential ($\Delta\psi_{mt}$) and oxygen consumption (ΔO_2). This phenotype corresponds to a metabolic switch from oxidative metabolism to the predominance of anaerobic bioenergetics. Use of trimetazidine (TMZ), Mdivi or DRP1 dominant negative (DRP1 K38A) prevents all these alterations, thus rescuing cells from both cell death and proliferation induction.

Mdivi, reversed not only the mitochondrial network fragmentation, but also the hypoxia induced decrease in the mitochondrial metabolism and the increased proliferative phenotype of hPASMC. Nonetheless, it has recently shown that Mdivi, in high doses, could also inhibit the mitochondrial complex I of the electron transport chain [33]. In sight of that, we additionally used a genetic approach to inhibit DRP1 function. In the same way as Mdivi, dominant negative DRP1 prevented the augmented cell proliferation induced by hypoxia. Altogether, these results and the previous observations by Marsboom et al. [42,43], highlights the importance of mitochondrial dynamics and specifically, DRP1, in the proliferation and metabolic shift observed during PAH.

TMZ has a complex effect on hypoxic cells that surpasses 3-ketoacyl-coA thiolase (3-KAT) inhibition and largely depends on the baseline metabolic status of cells. In cell types that rely on fatty acid oxidation as primary ATP source, such as cardiomyocytes, TMZ decreases oxygen consumption and ROS production [44], with a net anti-apoptotic effect through preservation of mitochondrial integrity [15,45], although this effect seems to depend on the TMZ dose [15]. In contrast, our data in hPASMC show that TMZ promotes mitochondrial metabolism and prevents the hypoxia-induced increase in DRP1 levels, thus increasing the GO/GLY ratio, likely due to its ability to shift Randle's cycle equilibrium favoring pyruvate oxidation. The potential mechanism involved may be through increasing mitochondrial Ca^{2+} concentration, which in turn augments the activity of Ca^{2+}-dependent citric acid cycle dehydrogenases [46]. Mounting evidence shows that intra-mitochondrial Ca^{2+} levels is largely dependent on mitochondrial connectivity, with a more elongated network being more efficient for Ca^{2+} uptake [47]. In accordance with that notion, not only TMZ, but also Mdivi restored mitochondrial function, along with decreasing the levels of key glycolytic markers, thus indicating the reversal of the GO/GLY shift induced by hypoxia.

Interestingly, all the metabolic changes that we observed in response to hypoxia were accompanied by increased proliferation, as evidenced by the nuclear pattern of Ki67, reinforcing the concept that in this cell line a decreased GO/GLY ratio leads to a shift towards a proliferative phenotype, as is seen in cancer cells. In this context, decreased MTS should be interpreted in the light of the metabolic changes above-mentioned that likely affect the rate of MTS reduction. In fact, MTS reduction is a marker of cell metabolism and not uniquely of cell proliferation. In our model, increased proliferation in hypoxic hPASMC is linked to a decrease in oxidative metabolism, thus decreasing the amount of reduced MTS per cell. Changes in the pH of the culture medium as well as diminished glucose availability due to higher number of cells may also contribute to the decrease in MTS levels observed in our cell model [48]. It is intriguing that TMZ induced a full reversion of MTS without eliciting a strong change in mitochondrial metabolism, evidenced by a partial recovery in oxygen consumption. This may be linked to increased NAD(P)H availability in response to increased activity of citric acid cycle enzymes [46,49] or decreased ROS production, thus increasing the concentration of sulfhydryl-containing compounds that can reduce MTS non-enzymatically [50]. In the case of Mdivi, it antagonized not only the hypoxia-induced metabolic shift, but also the proliferative response of hPASMC. Inhibition of DRP1 with Mdivi or mutant DRP1 both reversed the Ki67 fluorescence pattern, indicating that cells returned to their non-proliferative state. This is consistent with other work from our group, where thymidine incorporation was used as a marker for cell proliferation. There, both Mdivi and mutant DRP1 inhibited PDGF-BB-induced proliferation, in an *in vitro* model of vascular smooth muscle cells [23]. In sum, these observations imply a crucial role for DRP1, not only as a mitochondrial network regulator, but also as a controller of cell proliferation.

Another aspect of TMZ actions is its ability to regulate ROS production. Multiple studies show that oxidative stress is involved in the pathogenesis of both proliferative vasculopathy and right ventricular failure, two hallmarks of PAH [51]. Pharmacological inhibition of fatty acid oxidation by TMZ is known to increase mitochondrial ROS production in hypoxic murine PASMC [52], where changes in ROS levels act as signals for mitochondrial remodeling [53]. Although compelling, the study of ROS production as a signaling hub in hypoxic PASMC exceeds the scope of this study.

5. Conclusions

In summary, we have shown that preserving mitochondrial morphology and function during hypoxia prevents hPASMC metabolic shift towards glycolysis at the expense of mitochondrial oxidation. In this context, we pose TMZ as an efficient mitochondrial rescue agent, which precludes the establishment of a proliferative phenotype; one of the critical events associated with PAH onset and progression. Furthermore, this work shows that both pharmacological and genetic inhibition of

DRP1 recapitulates TMZ pro-oxidative and anti-proliferative effects, thereby suggesting that mitochondrial morphology acts as an upstream regulator of cell bioenergetics and vascular fate. Future work may help to elucidate the interplay among mitochondria, metabolism and cellular phenotype, and might provide novel pharmacological targets for PAH treatment.

Funding

This research was funded by Comisión Nacional de Investigación Científica y Tecnológica (CONICYT), Chile: FONDAP grant 15130011 (to S.L., P.F.C., H.E.V., V.P., M.C.), FONDECYT grants 1141198 (P.F.C.), 1150282 (V.P.), 1150359 (H.E.V.), 1140329 (M.C.), 1161156 to (S.L.); FONDECYT postdoctoral fellowship 3160226 (R.B.S.) and PAI Insertion Program grant 79150007 (V.P.).

Conflicts of interests

None declared.

Transparency Document

The Transparency document associated with this article can be found, in online version.

Acknowledgments

We thank Fidel Albornoz, Gindra Latorre and Sebastián Leiva for their excellent technical assistance.

Appendix A. Supplementary data

Supplementary data to this article can be found online at http://dx.doi.org/10.1016/j.bbadis.2017.07.018.

References

[1] V.V. McLaughlin, S.L. Archer, D.B. Badesch, R.J. Barst, H.W. Farber, J.R. Lindner, et al., ACCF/AHA 2009 expert consensus document on pulmonary hypertension: a report of the American College of Cardiology Foundation Task Force on Expert Consensus Documents and the American Heart Association: developed in collaboration with the American College of Chest Physicians, American Thoracic Society, Inc., and the Pulmonary Hypertension Association, Circulation, American Heart Association Journals (2009) 2250–2294, http://dx.doi.org/10.1161/CIRCULATIONAHA.109.192230.

[2] J. Grimminger, M. Richter, K. Tello, N. Sommer, H. Gall, H.A. Ghofrani, Thin air resulting in high pressure: mountain sickness and hypoxia-induced pulmonary hypertension, Can. Respir. J. 2017 (2017) 8381653, http://dx.doi.org/10.1155/2017/8381653.

[3] G. Sutendra, E.D. Michelakis, The metabolic basis of pulmonary arterial hypertension, Cell Metab. 19 (2014) 558–573, http://dx.doi.org/10.1016/j.cmet.2014.01.004.

[4] G. Sutendra, S. Bonnet, G. Rochefort, A. Haromy, K.D. Folmes, G.D. Lopaschuk, et al., Fatty acid oxidation and malonyl-CoA decarboxylase in the vascular remodeling of pulmonary hypertension, Sci. Transl. Med. 2 (2010) 44ra58, http://dx.doi.org/10.1126/scitranslmed.3001327.

[5] J. Kuzmicic, A. del Campo, C. López-Crisosto, P.E. Morales, C. Pennanen, R. Bravo-Sagua, et al., Mitochondrial dynamics: a potential new therapeutic target for heart failure, Rev. Esp. Cardiol. 64 (2011) 916–923, http://dx.doi.org/10.1016/j.recesp.2011.05.018.

[6] V. Parra, H. Verdejo, A. Campo, C. Pennanen, J. Kuzmicic, M. Iglewski, et al., The complex interplay between mitochondrial dynamics and cardiac metabolism, J. Bioenerg. Biomembr. 43 (2011) 47–51, http://dx.doi.org/10.1007/s10863-011-9332-0.

[7] A. Carlucci, L. Lignitto, A. Feliciello, Control of mitochondria dynamics and oxidative metabolism by cAMP, AKAPs and the proteasome, Trends Cell Biol. 18 (2008) 604–613, http://dx.doi.org/10.1016/j.tcb.2008.09.006.

[8] C. Vásquez-Trincado, I. Garcia-Carvajal, C. Pennanen, V. Parra, J.A. Hill, B.A. Rothermel, et al., Mitochondrial dynamics, mitophagy and cardiovascular disease, J. Physiol. 594 (2016) 509–525, http://dx.doi.org/10.1113/JP271301.

[9] H.M. McBride, M. Neuspiel, S. Wasiak, Mitochondria: more than just a powerhouse, Curr. Biol. 16 (2006) R551–R560, http://dx.doi.org/10.1016/j.cub.2006.06.054.

[10] M. Liesa, M. Palacín, A. Zorzano, Mitochondrial dynamics in mammalian health and disease, Physiol. Rev. 89 (2009) 799–845, http://dx.doi.org/10.1152/physrev.00030.2008.

[11] H. Chen, D.C. Chan, Emerging functions of mammalian mitochondrial fusion and fission, Hum. Mol. Genet. 14 (2005) R283–R289, http://dx.doi.org/10.1093/hmg/ddi270.

[12] C. Guarnieri, C. Muscari, Beneficial effects of trimetazidine on mitochondrial function and superoxide production in the cardiac muscle, Cardiovasc. Drugs Ther. 4 (Suppl. 4) (1990) 814–815.

[13] S. Allibardi, S.L. Chierchia, V. Margonato, G. Merati, G. Neri, G. Dell'Antonio, et al., Effects of trimetazidine on metabolic and functional recovery of postischemic rat hearts, Cardiovasc. Drugs Ther. 12 (1998) 543–549.

[14] M. Hamdan, S. Urien, H. Le Louet, J.P. Tillement, D. Morin, Inhibition of mitochondrial carnitine palmitoyltransferase-1 by a trimetazidine derivative, S-15176, Pharmacol. Res. 44 (2001) 99–104, http://dx.doi.org/10.1006/phrs.2001.0829.

[15] J. Kuzmicic, V. Parra, H.E. Verdejo, C. López-Crisosto, M. Chiong, L. García, et al., Trimetazidine prevents palmitate-induced mitochondrial fission and dysfunction in cultured cardiomyocytes, Biochem. Pharmacol. 91 (2014) 323–336, http://dx.doi.org/10.1016/j.bcp.2014.07.022.

[16] M.I. Hernández-Alvarez, J.C. Paz, D. Sebastián, J.P. Munoz, M. Liesa, J. Segalés, et al., Glucocorticoid modulation of mitochondrial function in hepatoma cells requires the mitochondrial fission protein Drp1, Antioxid. Redox Signal. 19 (2012) 366–378, http://dx.doi.org/10.1089/ars.2011.4269.

[17] A. del Campo, V. Parra, C. Vásquez-Trincado, T. Gutierrez, P.E. Morales, C. López-Crisosto, et al., Mitochondrial fragmentation impairs insulin-dependent glucose uptake by modulating Akt activity through mitochondrial Ca2 + uptake, Am. J. Physiol. Endocrinol. Metab. 306 (2014) E1–E13, http://dx.doi.org/10.1152/ajpendo.00146.2013.

[18] V. Parra, H.E. Verdejo, M. Iglewski, A. del Campo, R. Troncoso, D. Jones, et al., Insulin stimulates mitochondrial fusion and function in cardiomyocytes via the Akt-mTOR-NFκB-Opa-1 signaling pathway, Diabetes 63 (2014) 75–88, http://dx.doi.org/10.2337/db13-0340.

[19] T. Gutierrez, V. Parra, R. Troncoso, C. Pennanen, A. Contreras-Ferrat, C. Vásquez-Trincado, et al., Alteration in mitochondrial Ca2 + uptake disrupts insulin signaling in hypertrophic cardiomyocytes, Cell Commun. Signal 12 (2014) 68, http://dx.doi.org/10.1186/s12964-014-0068-4.

[20] M.W. Pfaffl, A new mathematical model for relative quantification in real-time RT-PCR, Nucleic Acids Res. 29 (2001) e45.

[21] A.C. McLellan, S.A. Phillips, P.J. Thornalley, Fluorimetric assay of D-lactate, Anal. Biochem. 206 (1992) 12–16.

[22] V. Parra, V. Eisner, M. Chiong, A. Criollo, F. Moraga, A. Garcia, et al., Changes in mitochondrial dynamics during ceramide-induced cardiomyocyte early apoptosis, Cardiovasc. Res. 77 (2008) 387–397, http://dx.doi.org/10.1093/cvr/cvm029.

[23] G. Torres, P.E. Morales, M. García-Miguel, I. Norambuena-Soto, B. Cartes-Saavedra, G. Vidal-Peña, et al., Glucagon-like peptide-1 inhibits vascular smooth muscle cell dedifferentiation through mitochondrial dynamics regulation, Biochem. Pharmacol. 104 (2016) 52–61, http://dx.doi.org/10.1016/j.bcp.2016.01.013.

[24] T. Yu, J.L. Robotham, Y. Yoon, Increased production of reactive oxygen species in hyperglycemic conditions requires dynamic change of mitochondrial morphology, Proc. Natl. Acad. Sci. U. S. A. 103 (2006) 2653–2658, http://dx.doi.org/10.1073/pnas.0511154103.

[25] P. Marambio, B. Toro, C. Sanhueza, R. Troncoso, V. Parra, H. Verdejo, et al., Glucose deprivation causes oxidative stress and stimulates aggresome formation and autophagy in cultured cardiac myocytes, Biochim. Biophys. Acta 1802 (2010) 509–518, http://dx.doi.org/10.1016/j.bbadis.2010.02.002.

[26] F. Paredes, V. Parra, N. Torrealba, M. Navarro-Marquez, D. Gatica, R. Bravo-Sagua, et al., HERPUD1 protects against oxidative stress-induced apoptosis through downregulation of the inositol 1,4,5-trisphosphate receptor, Free Radic. Biol. Med. 90 (2015) 206–218, http://dx.doi.org/10.1016/j.freeradbiomed.2015.11.024.

[27] G.L. Wang, B.H. Jiang, E.A. Rue, G.L. Semenza, Hypoxia-inducible factor 1 is a basic-helix-loop-helix-PAS heterodimer regulated by cellular O2 tension, Proc. Natl. Acad. Sci. U. S. A. 92 (1995) 5510–5514.

[28] N.V. Iyer, L.E. Kotch, F. Agani, S.W. Leung, E. Laughner, R.H. Wenger, et al., Cellular and developmental control of O2 homeostasis by hypoxia-inducible factor 1 alpha, Genes Dev. 12 (1998) 149–162.

[29] Z. Pedrozo, G. Sánchez, N. Torrealba, R. Valenzuela, C. Fernández, C. Hidalgo, et al., Calpains and proteasomes mediate degradation of ryanodine receptors in a model of cardiac ischemic reperfusion, Biochim. Biophys. Acta 1802 (2010) 356–362, http://dx.doi.org/10.1016/j.bbadis.2009.12.005.

[30] T. Scholzen, J. Gerdes, The Ki-67 protein: from the known and the unknown, J. Cell. Physiol. 182 (2000) 311–322, http://dx.doi.org/10.1002/(SICI)1097-4652(200003)182:3<311::AID-JCP1>3.0.CO;2-9.

[31] J. Bullwinkel, B. Baron-Lühr, A. Lüdemann, C. Wohlenberg, J. Gerdes, T. Scholzen, Ki-67 protein is associated with ribosomal RNA transcription in quiescent and proliferating cells, J. Cell. Physiol. 206 (2006) 624–635, http://dx.doi.org/10.1002/jcp.20494.

[32] A.P. Oyarzún, F. Westermeier, C. Pennanen, C. López-Crisosto, V. Parra, C. Sotomayor-Flores, et al., FK866 compromises mitochondrial metabolism and adaptive stress responses in cultured cardiomyocytes, Biochem. Pharmacol. 98 (2015) 92–101, http://dx.doi.org/10.1016/j.bcp.2015.08.097.

[33] E.A. Bordt, P. Clerc, B.A. Roelofs, A.J. Saladino, L. Tretter, V. Adam-Vizi, et al., The putative Drp1 inhibitor mdivi-1 is a reversible mitochondrial complex I inhibitor that modulates reactive oxygen species, Dev. Cell 40 (2017) 583–594.e6, http://dx.doi.org/10.1016/j.devcel.2017.02.020.

[34] S.L. Archer, Y.H. Fang, J.J. Ryan, L. Piao, Metabolism and bioenergetics in the right ventricle and pulmonary vasculature in pulmonary hypertension, Pulm. Circ. 3 (2013) 144–152, http://dx.doi.org/10.4103/2045-8932.109960.

[35] P. Dromparis, R. Paulin, T.H. Stenson, A. Haromy, G. Sutendra, E.D. Michelakis,

Attenuating endoplasmic reticulum stress as a novel therapeutic strategy in pulmonary hypertension, Circulation 127 (2013) 115–125, http://dx.doi.org/10.1161/CIRCULATIONAHA.112.133413.
[36] J. Ryan, A. Dasgupta, J. Huston, K.-H. Chen, S.L. Archer, Mitochondrial dynamics in pulmonary arterial hypertension, J. Mol. Med. 93 (2015) 229–242, http://dx.doi.org/10.1007/s00109-015-1263-5.
[37] G. Kanfer, B. Kornmann, Dynamics of the mitochondrial network during mitosis, Biochem. Soc. Trans. 44 (2016) 510–516, http://dx.doi.org/10.1042/BST20150274.
[38] K. Veitch, L. Maisin, L. Hue, Trimetazidine effects on the damage to mitochondrial functions caused by ischemia and reperfusion, Am. J. Cardiol. 76 (1995) 25B–30B.
[39] C. Guarnieri, C. Muscari, Beneficial effects of trimetazidine on mitochondrial function and superoxide production in the cardiac muscle of monocrotaline-treated rats, Biochem. Pharmacol. 37 (1988) 4685–4688.
[40] P. Monteiro, A.I. Duarte, L.M. Gonçalves, A. Moreno, L.A. Providência, Protective effect of trimetazidine on myocardial mitochondrial function in an ex-vivo model of global myocardial ischemia, Eur. J. Pharmacol. 503 (2004) 123–128, http://dx.doi.org/10.1016/j.ejphar.2004.09.003.
[41] E. Schrepfer, L. Scorrano, Mitofusins, from mitochondria to metabolism, Mol. Cell 61 (2016) 683–694, http://dx.doi.org/10.1016/j.molcel.2016.02.022.
[42] G. Marsboom, P.T. Toth, J.J. Ryan, Z. Hong, X. Wu, Y.H. Fang, et al., Dynamin-related protein 1-mediated mitochondrial mitotic fission permits hyperproliferation of vascular smooth muscle cells and offers a novel therapeutic target in pulmonary hypertension, Circ. Res. 110 (2012) 1484–1497, http://dx.doi.org/10.1161/CIRCRESAHA.111.263848.
[43] M.S. Wolin, Novel role for the regulation of mitochondrial fission by hypoxia inducible factor-1α in the control of smooth muscle remodeling and progression of pulmonary hypertension, Circ. Res. 110 (2012) 1395–1397, http://dx.doi.org/10.1161/CIRCRESAHA.112.270801.
[44] C. Guarnieri, C. Muscari, Effect of trimetazidine on mitochondrial function and oxidative damage during reperfusion of ischemic hypertrophied rat myocardium, Pharmacology 46 (1993) 324–331.
[45] L. Argaud, L. Gomez, O. Gateau-Roesch, E. Couture-Lepetit, J. Loufouat, D. Robert, et al., Trimetazidine inhibits mitochondrial permeability transition pore opening and prevents lethal ischemia-reperfusion injury, J. Mol. Cell. Cardiol. 39 (2005) 893–899, http://dx.doi.org/10.1016/j.yjmcc.2005.09.012.
[46] C. Guarnieri, C. Finelli, M. Zini, C. Muscari, Effects of trimetazidine on the calcium transport and oxidative phosphorylation of isolated rat heart mitochondria, Basic Res. Cardiol. 92 (1997) 90–95.
[47] R. Bravo-Sagua, V. Parra, C. López-Crisosto, P. Díaz, A.F.G. Quest, S. Lavandero, Calcium transport and signaling in mitochondria, Compr. Physiol. 7 (2017) 623–634, http://dx.doi.org/10.1002/cphy.c160013.
[48] G.S. Sittampalam, N.P. Coussens, H. Nelson, M. Arkin, D. Auld, C. Austin, et al., Cell Viability Assays (2004).
[49] J.G. McCormack, R.M. Denton, Mitochondrial Ca2 + transport and the role of intramitochondrial Ca2 + in the regulation of energy metabolism, Dev. Neurosci. 15 (1993) 165–173.
[50] J.L. York, L.C. Maddox, P. Zimniak, T.E. McHugh, D.F. Grant, Reduction of MTT by glutathione S-transferase, BioTechniques 25 (1998) 626–628.
[51] Y.J. Suzuki, R.H. Steinhorn, M.T. Gladwin, Antioxidant therapy for the treatment of pulmonary hypertension, Antioxid. Redox Signal. 18 (2013) 1723–1726, http://dx.doi.org/10.1089/ars.2013.5193.
[52] G. Sutendra, P. Dromparis, P. Wright, S. Bonnet, A. Haromy, Z. Hao, et al., The role of Nogo and the mitochondria-endoplasmic reticulum unit in pulmonary hypertension, Sci. Transl. Med. 3 (2011) 88ra55, http://dx.doi.org/10.1126/scitranslmed.3002194.
[53] S. Iqbal, D.A. Hood, Oxidative stress-induced mitochondrial fragmentation and movement in skeletal muscle myoblasts, Am. J. Physiol. Cell Physiol. 306 (2014) C1176–C1183, http://dx.doi.org/10.1152/ajpcell.00017.2014.